

CLNS 98/1545
 CLEO 98-5
 May 24, 2021

Measurement of the Mass Splittings between the $b\bar{b}$ $\chi_{b,J}(1P)$ States

CLEO Collaboration
 (May 24, 2021)

Abstract

We present new measurements of photon energies and branching fractions for the radiative transitions: $\Upsilon(2S) \rightarrow \gamma \chi_{b(J=0,1,2)}(1P)$. The masses of the χ_b states are determined from the measured radiative photon energies. The ratio of mass splittings between the χ_b substates, $r \equiv (M_{J=2} - M_{J=1})/(M_{J=1} - M_{J=0})$, with M the χ_b mass, provides information on the nature of the $b\bar{b}$ confining potential. We find $r(1P) = 0.54 \pm 0.02 \pm 0.02$. This value is in conflict with the previous world average, but more consistent with the theoretical expectation that $r(1P) < r(2P)$; i.e., that this mass splittings ratio is smaller for the $\chi_b(1P)$ states than for the $\chi_b(2P)$ states.

K. W. Edwards,¹ A. Bellerive,² R. Janicek,² D. B. MacFarlane,² P. M. Patel,²
 A. J. Sadoff,³ R. Ammar,⁴ P. Baringer,⁴ A. Bean,⁴ D. Besson,⁴ D. Coppage,⁴ C. Darling,⁴
 R. Davis,⁴ S. Kotov,⁴ I. Kravchenko,⁴ N. Kwak,⁴ L. Zhou,⁴ S. Anderson,⁵ Y. Kubota,⁵
 S. J. Lee,⁵ J. J. O'Neill,⁵ R. Poling,⁵ T. Riehle,⁵ A. Smith,⁵ M. S. Alam,⁶ S. B. Athar,⁶
 Z. Ling,⁶ A. H. Mahmood,⁶ S. Timm,⁶ F. Wappler,⁶ A. Anastassov,⁷ J. E. Duboscq,⁷
 D. Fujino,^{7,1} K. K. Gan,⁷ T. Hart,⁷ K. Honscheid,⁷ H. Kagan,⁷ R. Kass,⁷ J. Lee,⁷
 H. Schwarthoff,⁷ M. B. Spencer,⁷ M. Sung,⁷ A. Undrus,^{7,2} A. Wolf,⁷ M. M. Zoeller,⁷
 S. J. Richichi,⁸ H. Severini,⁸ P. Skubic,⁸ M. Bishai,⁹ J. Fast,⁹ J. W. Hinson,⁹ N. Menon,⁹
 D. H. Miller,⁹ E. I. Shibata,⁹ I. P. J. Shipsey,⁹ M. Yurko,⁹ S. Glenn,¹⁰ Y. Kwon,^{10,3}
 A. L. Lyon,¹⁰ S. Roberts,¹⁰ E. H. Thorndike,¹⁰ C. P. Jessop,¹¹ K. Lingel,¹¹ H. Marsiske,¹¹
 M. L. Perl,¹¹ V. Savinov,¹¹ D. Ugolini,¹¹ X. Zhou,¹¹ T. E. Coan,¹² V. Fadeyev,¹²
 I. Korolkov,¹² Y. Maravin,¹² I. Narsky,¹² V. Shelkov,¹² J. Staeck,¹² R. Stroynowski,¹²
 I. Volobouev,¹² J. Ye,¹² M. Artuso,¹³ F. Azfar,¹³ A. Efimov,¹³ M. Goldberg,¹³ D. He,¹³
 S. Kopp,¹³ G. C. Moneti,¹³ R. Mountain,¹³ S. Schuh,¹³ T. Skwarnicki,¹³ S. Stone,¹³
 G. Viehhauser,¹³ J. C. Wang,¹³ X. Xing,¹³ J. Bartelt,¹⁴ S. E. Csorna,¹⁴ V. Jain,^{14,4}
 K. W. McLean,¹⁴ S. Marka,¹⁴ R. Godang,¹⁵ K. Kinoshita,¹⁵ I. C. Lai,¹⁵ P. Pomianowski,¹⁵
 S. Schrenk,¹⁵ G. Bonvicini,¹⁶ D. Cinabro,¹⁶ R. Greene,¹⁶ L. P. Perera,¹⁶ G. J. Zhou,¹⁶
 M. Chadha,¹⁷ S. Chan,¹⁷ G. Eigen,¹⁷ J. S. Miller,¹⁷ M. Schmidtler,¹⁷ J. Urheim,¹⁷
 A. J. Weinstein,¹⁷ F. Würthwein,¹⁷ D. W. Bliss,¹⁸ D. E. Jaffe,¹⁸ G. Masek,¹⁸ H. P. Paar,¹⁸
 S. Prell,¹⁸ V. Sharma,¹⁸ D. M. Asner,¹⁹ J. Gronberg,¹⁹ T. S. Hill,¹⁹ D. J. Lange,¹⁹
 R. J. Morrison,¹⁹ H. N. Nelson,¹⁹ T. K. Nelson,¹⁹ D. Roberts,¹⁹ B. H. Behrens,²⁰
 W. T. Ford,²⁰ A. Gritsan,²⁰ J. Roy,²⁰ J. G. Smith,²⁰ J. P. Alexander,²¹ R. Baker,²¹
 C. Bebek,²¹ B. E. Berger,²¹ K. Berkelman,²¹ K. Bloom,²¹ V. Boisvert,²¹ D. G. Cassel,²¹
 D. S. Crowcroft,²¹ M. Dickson,²¹ S. von Dombrowski,²¹ P. S. Drell,²¹ K. M. Ecklund,²¹
 R. Ehrlich,²¹ A. D. Foland,²¹ P. Gaidarev,²¹ R. S. Galik,²¹ L. Gibbons,²¹ B. Gittelman,²¹
 S. W. Gray,²¹ D. L. Hartill,²¹ B. K. Heltsley,²¹ P. I. Hopman,²¹ J. Kandaswamy,²¹
 D. L. Kreinick,²¹ T. Lee,²¹ Y. Liu,²¹ N. B. Mistry,²¹ C. R. Ng,²¹ E. Nordberg,²¹ M. Ogg,^{21,5}
 J. R. Patterson,²¹ D. Peterson,²¹ D. Riley,²¹ A. Soffer,²¹ B. Valant-Spaight,²¹ C. Ward,²¹
 M. Athanas,²² P. Avery,²² C. D. Jones,²² M. Lohner,²² S. Patton,²² C. Prescott,²²
 J. Yelton,²² J. Zheng,²² G. Brandenburg,²³ R. A. Briere,²³ A. Ershov,²³ Y. S. Gao,²³
 D. Y.-J. Kim,²³ R. Wilson,²³ H. Yamamoto,²³ T. E. Browder,²⁴ Y. Li,²⁴ J. L. Rodriguez,²⁴
 T. Bergfeld,²⁵ B. I. Eisenstein,²⁵ J. Ernst,²⁵ G. E. Gladding,²⁵ G. D. Gollin,²⁵ R. M. Hans,²⁵
 E. Johnson,²⁵ I. Karliner,²⁵ M. A. Marsh,²⁵ M. Palmer,²⁵ M. Selen,²⁵ and J. J. Thaler²⁵

¹Carleton University, Ottawa, Ontario, Canada K1S 5B6

¹Permanent address: Lawrence Livermore National Laboratory, Livermore, CA 94551.

²Permanent address: BINP, RU-630090 Novosibirsk, Russia.

³Permanent address: Yonsei University, Seoul 120-749, Korea.

⁴Permanent address: Brookhaven National Laboratory, Upton, NY 11973.

⁵Permanent address: University of Texas, Austin TX 78712.

and the Institute of Particle Physics, Canada

²McGill University, Montréal, Québec, Canada H3A 2T8

and the Institute of Particle Physics, Canada

³Ithaca College, Ithaca, New York 14850

⁴University of Kansas, Lawrence, Kansas 66045

⁵University of Minnesota, Minneapolis, Minnesota 55455

⁶State University of New York at Albany, Albany, New York 12222

⁷Ohio State University, Columbus, Ohio 43210

⁸University of Oklahoma, Norman, Oklahoma 73019

⁹Purdue University, West Lafayette, Indiana 47907

¹⁰University of Rochester, Rochester, New York 14627

¹¹Stanford Linear Accelerator Center, Stanford University, Stanford, California 94309

¹²Southern Methodist University, Dallas, Texas 75275

¹³Syracuse University, Syracuse, New York 13244

¹⁴Vanderbilt University, Nashville, Tennessee 37235

¹⁵Virginia Polytechnic Institute and State University, Blacksburg, Virginia 24061

¹⁶Wayne State University, Detroit, Michigan 48202

¹⁷California Institute of Technology, Pasadena, California 91125

¹⁸University of California, San Diego, La Jolla, California 92093

¹⁹University of California, Santa Barbara, California 93106

²⁰University of Colorado, Boulder, Colorado 80309-0390

²¹Cornell University, Ithaca, New York 14853

²²University of Florida, Gainesville, Florida 32611

²³Harvard University, Cambridge, Massachusetts 02138

²⁴University of Hawaii at Manoa, Honolulu, Hawaii 96822

²⁵University of Illinois, Urbana-Champaign, Illinois 61801

I. INTRODUCTION

The Υ particles (bound systems of heavy bottom–anti-bottom quarks) play an important role in studies of strong interactions. The bottom–anti-bottom pair creates a positronium-like system bound by strong interactions. Because the Υ system is nearly non-relativistic ($\beta^2 \approx 0.08$), theory can start from a relatively simple non-relativistic potential model and add relativistic terms as next-order corrections to describe the Υ mass-spectrum, as well as the partial widths for the transitions expected within the bottomonium system. Relativistic effects as a result of spin-orbit and tensor interactions generate fine splittings; hyperfine splittings arise from spin-spin interactions. Potential models predict electric dipole transitions $\Upsilon(2S) \rightarrow \gamma \chi_{b,J}(1P)$ with rates proportional to $(2J+1)E_\gamma^3$, with E_γ the photon energy. These transitions have already been investigated in four experiments – CUSB [1], CLEO [2], Crystal Ball [3] and ARGUS [4] – by measuring the energy distribution of transition photons detected inclusively in multi-hadronic events: $\Upsilon(2S) \rightarrow \gamma \chi_{b,J}(1P)$; $\chi_{b,J}(1P) \rightarrow$ hadrons. The exclusive radiative cascade transitions, $\Upsilon(2S) \rightarrow \gamma \chi_{b,J}(1P)$; $\chi_{b,J}(1P) \rightarrow \gamma \Upsilon(1S)$, in which the $\Upsilon(1S)$ is tagged by its decay to dileptons, were measured by the CUSB [5] and Crystal Ball [6] experiments.

In the present analysis, we have used the inclusive method to study the radiative photon transitions between the $\Upsilon(2S)$ and the $\chi_{b,J}(1P)$ and measure the fine structure of the P states, which can be characterized by the ratio of mass splittings within the triplet: $r \equiv (M_{J=2} - M_{J=1})/(M_{J=1} - M_{J=0})$. The ratio of mass splittings measured in $\Upsilon(3S)$ radiative transitions to the $\chi_{b,J}(2P)$ triplet is $r(2P) = 0.58 \pm 0.01$ [7]. Phenomenologically, the parameter r gives information on the Lorentz transformation properties of the $b\bar{b}$ confining potential; different predictions for r result from different assumptions about the relative vector and scalar contributions. The tabulated world average for the ratio of mass splittings measured for the $\chi_{b,J}(1P)$ triplet is $r(1P) = 0.65 \pm 0.03$ [8], corresponding to $r(2P) < r(1P)$, opposite to most model predictions [8].

II. DATA SAMPLE AND ANALYSIS DESCRIPTION

These data were obtained with the CLEO II detector [9] at the Cornell Electron Storage Ring, CESR, corresponding to an integrated luminosity of 73.6 pb^{-1} at the $\Upsilon(2S)$ energy. Based on the number of hadronic events measured at this energy, we determine that this luminosity is equivalent to a total number of $(488 \pm 18) \cdot 10^3$ produced $\Upsilon(2S)$ events. The advantage of the present analysis over previous analyses lies primarily in the high segmentation of the CLEO II calorimeter, which offers improved resolution of individual photon showers, with excellent solid angle coverage.

Candidate events are required to have at least three observed charged tracks in the event, with a total visible energy greater than the single electron (or positron) beam energy. Additional criteria are imposed to minimize contamination to our photon spectrum from non-hadronic events, such as beam-gas, beam-wall, or two-photon collisions [10]. We note that such backgrounds contribute only a smooth background to our observed photon energy spectrum.

A. Measurement of Photon Transition Energies

Only photons from the barrel region ($|\cos \theta_\gamma| < 0.7$, with θ_γ the polar angle of the shower) are considered in this analysis. The fractional energy resolution for photons in the barrel region

of the calorimeter ($\sigma_E \approx 5\%$ for $E_\gamma = 130$ MeV) is approximately twice as good as in the endcap regions. Photon candidates are required to be well separated from charged tracks and other photon candidates in the same event. The lateral shower shape is required to be consistent with that expected from a true photon, and inconsistent with the energy deposition patterns expected for charged particles. Showers from “hot spots” in the calorimeter are flagged on a run-by-run basis and eliminated from consideration as inclusive photon candidates.

The photon energy scale is set by a three-stage calorimeter calibration procedure [9,10]. Pulsing of the readout electronics enables determination of the pedestals and gains characteristic of each channel, independent of the crystal light output. The energy calibrations for individual crystals are then calculated using reconstructed showers matched to beam-energy electrons in Bhabha events; the factors which convert normalized crystal light output to energy deposition, one per crystal, are obtained by minimizing the r.m.s. width of the electron shower energy distribution and constraining it to peak at the beam energy. The third and final stage of calibration guarantees that any monochromatic photon energy spectrum peaks at the incident photon energy, effectively correcting for any non-linearity in crystal response, shower leakage from the cesium iodide, or bias in the reconstruction algorithm. This absolute energy calibration selects photon candidates that can be kinematically constrained, using radiative Bhabha ($ee\gamma$), $\gamma\gamma$ ($\gamma\gamma\gamma$), and muon pair ($\mu\mu\gamma$) events for photons above 0.5 GeV and π^0 ’s below 2.5 GeV. Most relevant to this analysis is the π^0 calibration, which requires consistency between the observed $\pi^0 \rightarrow \gamma\gamma$ mass peak and the expected mass. The π^0 calibration accounts for the contributions to the observed π^0 mass lineshape from energy-dependent shower angle and energy resolutions of both its constituent photons. The correction amounts to $\sim 1\%$ near 100 MeV, and varies slowly and continuously with energy. The $ee\gamma$, $\mu\mu\gamma$, $\gamma\gamma\gamma$, and π^0 samples yield compatible corrections in the energy regions where they can be compared with one another. For the energy regime in this analysis we assess the uncertainty in the overall absolute energy scale to be $\pm 0.4\%$.

After applying all event selection requirements and photon criteria, we obtain the inclusive photon spectrum shown in Figure 1, with a fit to signal plus background overlaid. Three enhancements are visible in this distribution above a smooth background. We attribute the lower energy photon peak to $\Upsilon(2S) \rightarrow \gamma\chi_{b,2}(1P)$, the middle peak to $\Upsilon(2S) \rightarrow \gamma\chi_{b,1}(1P)$, and the highest energy peak to the $\Upsilon(2S) \rightarrow \gamma\chi_{b,0}(1P)$ transition. The smooth background is primarily due to $\pi^0 \rightarrow \gamma\gamma$ photons, as well as non-photon showers which passed the photon selection criteria. We fit this background shape using a third order polynomial.

The signal shape is parameterized using a functional form originally used by the Crystal Ball collaboration [11]. This is a nearly Gaussian distribution with a tail at lower energies to take into account longitudinal and transverse shower leakage in the calorimeter. The expected ratios of the line widths (i.e., the shape of the resolution curve as a function of photon energy) are fixed from Monte Carlo simulations; the width of one of the lines ($J=1$) is allowed to float in the fit. Since the intrinsic widths of the $\chi_{b,J}(1P)$ states are expected to be of order ≤ 1 MeV, the experimental resolution should dominate the observed line width. The aggregate signal function therefore has seven free parameters: the three line positions, their areas, and the energy resolution of the middle photon line. The spectrum of photon candidates after the third order polynomial is subtracted is shown in Figure 2a), with the aggregate signal function overlaid. The results of the fit are given in Table I (only statistical errors are presented). In Figure 2b), we have superimposed upon the background-subtracted spectrum the signals that would be expected, using the presently tabulated values for the masses of the $\chi_{b,J}(1P)$ states [7]. It is clear that this results in an inferior fit.

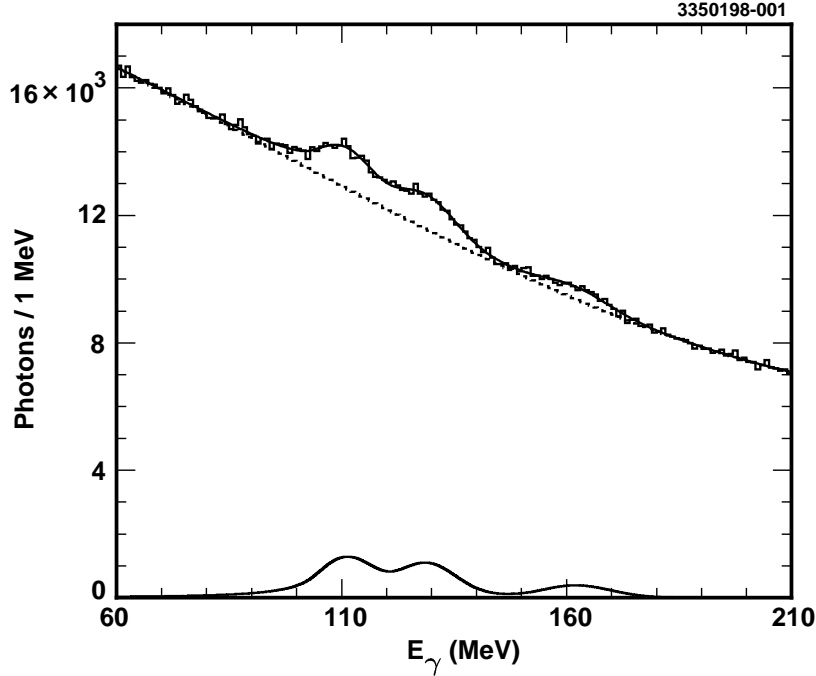


FIG. 1. Fit to the inclusive spectrum of photon candidates for the $\Upsilon(2S)$ data set. Also shown is the signal function used in the fit.

Our background-subtracted data are obviously incompatible with the presently tabulated $\chi_{b,J}(1P)$ masses. From the fit in Fig. 2a), $r(1P)$ is determined to be 0.54 ± 0.02 (statistical error only).

TABLE I. Energies, raw yields (from fit to data photon spectrum) and efficiencies (from Monte Carlo simulations, and including J -dependent geometric acceptances) for $\Upsilon(2S) \rightarrow \gamma \chi_{b,J}(1P)$ transitions. Errors shown are statistical only.

Transition	E_γ (MeV)	Yield (N_γ)	Efficiency (%)
$J = 2$	110.8 ± 0.3	20723 ± 1436	57.1 ± 5.2
$J = 1$	128.8 ± 0.4	20806 ± 1466	52.4 ± 7.1
$J = 0$	162.0 ± 0.8	8637 ± 1274	61.8 ± 5.9

B. Branching Fractions

We use a GEANT-based, full CLEO II Monte Carlo simulation to determine the photon finding efficiency for each transition line, as presented in Table I. The geometric acceptance is calculated for each transition using the appropriate polar angular distributions for transitions to the $J = 2$ ($dN/d\cos\theta_\gamma \propto 1 + \frac{1}{13}\cos^2\theta_\gamma$), $J = 1$ ($dN/d\cos\theta_\gamma \propto 1 + \cos^2\theta_\gamma$), and $J = 0$ ($dN/d\cos\theta_\gamma \propto 1 - \frac{1}{3}\cos^2\theta_\gamma$) states, respectively. We use the acceptance appropriate for each transition (Table I) to calculate the branching fractions from the $\Upsilon(2S)$ to the $\chi_{b,J}(1P)$ triplet states (Table III).

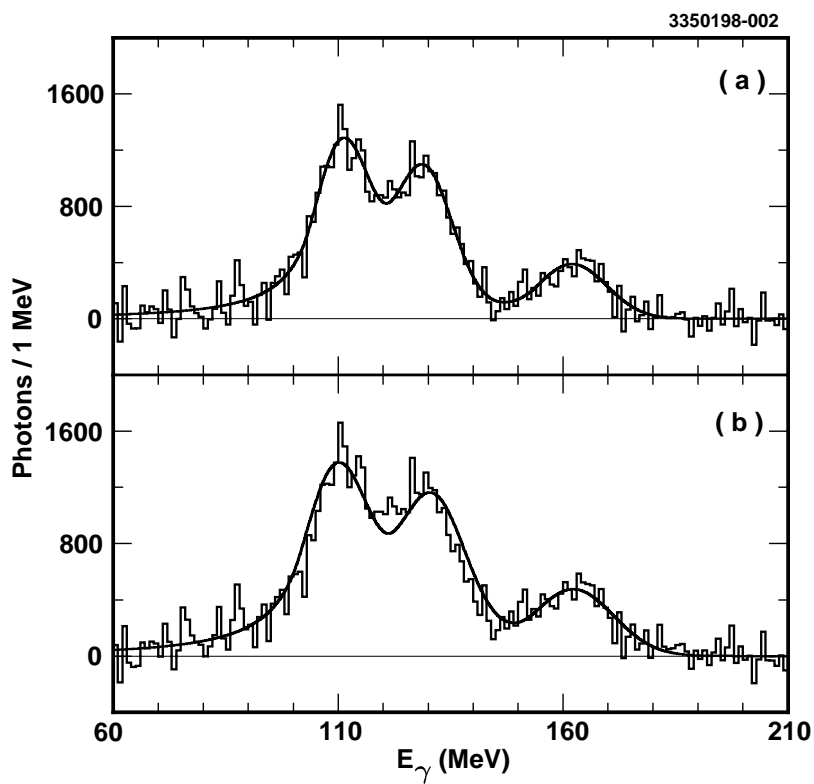


FIG. 2. Background subtracted photon energy spectrum, showing results of a free fit (top curve overlaying the histogram), and also overlay of the signal function curve obtained by constraining the masses of the $\chi_{b,J}(1P)$ masses to their previously tabulated values (bottom).

C. Systematic Uncertainties and Cross-checks

In addition to the systematic error due to the calorimeter calibration, primary systematic errors are due to event and photon selection and the signal extraction procedure, as summarized in Table II. The photon selection systematic is evaluated by remeasuring the photon spectrum using different definitions of ‘photons’. We estimate the signal extraction systematic by using a variety of signal parameterizations (using a bifurcated Gaussian rather than the Crystal Ball line shape, e.g.) and different parameterizations for the background under the signal. The larger overall systematic error for the $J = 0$ line is attributable to the closer proximity of the minimum ionizing peak for this line compared to the two lower energy lines (and hence, greater sensitivity to photon selection requirements designed to suppress showers from charged tracks) and a greater uncertainty in the extrapolated energy resolution at this energy.

TABLE II. Evaluation of the total systematic errors.

Uncertainty in:	Calibration error	selection	fitting	number of $\Upsilon(2S)$ produced	total
$J = 2$ line position (MeV)	0.40	0.27	0.38	-	0.6
$J = 1$ line position (MeV)	0.42	0.26	0.31	-	0.6
$J = 0$ line position (MeV)	0.45	0.62	0.93	-	1.2
r	0.001	0.012	0.021	-	0.02
$\mathcal{B}(\Upsilon(2S) \rightarrow \gamma \chi_{b,2})$ (%)	-	4.6	5.9	3.7	8.3
$\mathcal{B}(\Upsilon(2S) \rightarrow \gamma \chi_{b,1})$ (%)	-	5.9	7.5	3.7	10.2
$\mathcal{B}(\Upsilon(2S) \rightarrow \gamma \chi_{b,0})$ (%)	-	10.3	11.6	3.7	15.9
$\frac{ \langle \chi_{b,2}(1P) R 2S \rangle ^2}{ \langle \chi_{b,1}(1P) R 2S \rangle ^2}$	-	0.055	0.096	-	0.11
$\frac{ \langle \chi_{b,0}(1P) R 2S \rangle ^2}{ \langle \chi_{b,1}(1P) R 2S \rangle ^2}$	-	0.041	0.255	-	0.26

As a cross-check on the extracted value of r , we have conducted a parallel analysis, in which we search for photons in the ‘exclusive’ mode. In this case, we fully reconstruct the decay chain: $\Upsilon(2S) \rightarrow \chi_{b,J}(1P)\gamma$; $\chi_{b,J}(1P) \rightarrow \gamma \Upsilon(1S)$; $\Upsilon(1S) \rightarrow l^+l^-$, for which l^+l^- is e^+e^- or $\mu^+\mu^-$. This very distinctive final state topology consists of two leptons and two photons. Unfortunately, due to the very small branching fraction for $\chi_{b,0}(1P) \rightarrow \gamma \Upsilon(1S)$, these exclusive events cannot be used to completely determine $r(1P)$. Nevertheless, we find that the measured mass difference between the $J = 2$ and $J = 1$ states from our exclusive data ($\Delta M = 129.9 \pm 0.7 - 111.0 \pm 1.1$ MeV = 18.9 ± 1.3 MeV, statistical errors only) is in agreement with the mass difference measured in the inclusive mode ($\Delta M = 18.0 \pm 1.0$ MeV, as computed from Table III). We can also combine the masses observed for the $J = 2$ and $J = 1$ states in the exclusive mode with the mass measured for the $J = 0$ state in the inclusive mode to obtain a value of r' ; the superscript here indicates that this quantity is derived from a combination of the exclusive and the inclusive measurements. We obtain $r' = 0.59 \pm 0.05$ (statistical errors only), consistent with the value we obtained from the inclusive data. We do not include these exclusive results in our final determination of $r(1P)$ owing to their relatively small statistical weight compared to the inclusive sample.

D. Comparison with Previous Experimental Results

Table III summarizes the results for the photon energies from our inclusive analysis and compares our results with the present Particle Data Group averages. We have also tabulated the $\chi_{b,J}(1P)$ masses inferred from our measured photon energies. Table III similarly compares our results for the branching fractions with previous measurements. We find $r(1P)$ to be $0.54 \pm 0.02 \pm 0.02$, inconsistent with the previous world average of 0.65 ± 0.03 . Note that $r(1P)$ is insensitive to an overall miscalibration of the photon energy scale.

TABLE III. $\Upsilon(2S) \rightarrow \gamma X$ Transition energies and branching fractions (\mathcal{B}).

Transition	E_γ (This Expt.) (MeV)	E_γ PDG [7] (MeV)	$M(\chi_{b,J})(1P)$ (This Expt.) (MeV)	\mathcal{B} (This Expt.) (%)	PDG [7] (%)
$J = 2$	$110.8 \pm 0.3 \pm 0.6$	109.6 ± 0.6	$9912.5 \pm 0.3 \pm 0.6$	$7.4 \pm 0.5 \pm 0.6$	6.6 ± 0.9
$J = 1$	$128.8 \pm 0.4 \pm 0.6$	130.6 ± 0.7	$9894.5 \pm 0.4 \pm 0.6$	$6.9 \pm 0.5 \pm 0.7$	6.7 ± 0.9
$J = 0$	$162.0 \pm 0.8 \pm 1.2$	162.3 ± 1.3	$9863.0 \pm 0.8 \pm 1.2$	$3.4 \pm 0.5 \pm 0.5$	4.3 ± 1.0

The widths for the electric dipole transitions $\Upsilon(2S) \rightarrow \gamma \chi_{b,J}(1P)$ are given in terms of the characteristic interquark separation R by:

$$\Gamma_{E1} = \mathcal{B} \Gamma_{tot} = \frac{4}{27} \alpha e_b^2 E_\gamma^3 (2J+1) |\langle 1P | R | 2S \rangle|^2,$$

In this equation, α is the electromagnetic coupling constant, e_b is the charge of b quark, and $\langle 1P | R | 2S \rangle$ is the matrix element. By averaging over the transitions to all three $\chi_{b,J}(1P)$ states and using $\Gamma_{tot}(2S) = (44.0 \pm 7.0)$ keV [7], we find $\langle 1P | R | 2S \rangle = (1.88 \pm 0.12)$ GeV $^{-1}$, in which the error includes both statistical and systematic errors. This can be compared to the world average $\langle 1P | R | 2S \rangle = (1.9 \pm 0.2)$ GeV $^{-1}$ [8].

By determining the ratios of the transition widths for states having different total angular momentum J , we can cancel the uncertainty due to the total $\Upsilon(2S)$ width. Ratios of the squared matrix element for different J values are equal to ratios of the quantity $\Gamma_{E1}/(E_\gamma^3(2J+1))$. Table IV presents our experimental results and the previous world average for ratios of $\Gamma_{E1}/(E_\gamma^3(2J+1))$. Theoretically these ratios are expected to be 1.0 in the non-relativistic limit. Spin dependence of the matrix element is introduced by relativistic corrections. Although calculations vary, all models predict that the J-dependent corrections follow: $|\langle \chi_{b,2}(1P) | R | 2S \rangle|^2 > |\langle \chi_{b,1}(1P) | R | 2S \rangle|^2 > |\langle \chi_{b,0}(1P) | R | 2S \rangle|^2$ [8].

TABLE IV. Ratios of $\Gamma_{E1}/(E_\gamma^3(2J+1))$.

	$\frac{ \langle \chi_{b,2}(1P) R 2S \rangle ^2}{ \langle \chi_{b,1}(1P) R 2S \rangle ^2}$	$\frac{ \langle \chi_{b,0}(1P) R 2S \rangle ^2}{ \langle \chi_{b,1}(1P) R 2S \rangle ^2}$
This Experiment	$1.02 \pm 0.06 \pm 0.11$	$0.75 \pm 0.09 \pm 0.26$
Previous World Average [8]	0.92 ± 0.11	0.95 ± 0.16

III. SUMMARY

Based on the inclusive measurement of photon energies taken from $\Upsilon(2S)$ data, we have measured the branching fractions from the $\Upsilon(2S)$ state to the $\chi_{b,J}$ triplet, as well as the masses of the

states in the triplet. We find the ratio of mass splittings, $r(1P) \equiv (M_{J=2} - M_{J=1}) / (M_{J=1} - M_{J=0}) = 0.54 \pm 0.02 \pm 0.02$, substantially lower than the previous world average, but consistent with the expectation that $r(1P) < r(2P)$.

IV. ACKNOWLEDGMENTS

We gratefully acknowledge the effort of the CESR staff in providing us with excellent luminosity and running conditions. This work was supported by the National Science Foundation, the U.S. Department of Energy, Research Corporation, the Natural Sciences and Engineering Research Council of Canada, the A.P. Sloan Foundation, the Swiss National Science Foundation, and the Alexander von Humboldt Stiftung.

REFERENCES

- [1] CUSB Collaboration, C. Klopfenstein *et al.*, Phys. Rev. Lett. **51**, 160 (1983).
- [2] CLEO Collaboration, P. Haas *et al.*, Phys. Rev. Lett. **52**, 799 (1984).
- [3] Crystal Ball Collaboration, R. Nernst *et al.*, Phys. Rev. Lett. **54**, 2195 (1985).
- [4] ARGUS Collaboration, H. Albrecht *et al.*, Phys. Lett. **B160**, 331 (1985).
- [5] CUSB Collaboration, F. Pauss *et al.*, Phys. Lett. **B130**, 439 (1983).
- [6] Crystal Ball Collaboration, W. Walk *et al.*, Phys. Rev. **D34**, 2611 (1986).
- [7] R. M. Barnett *et al.*, Particle Data Group, Phys. Rev. **D54**, 19 (1996).
- [8] D. Besson and T. Skwarnicki, Ann. Rev. Nucl. Part. Sci. **43**, 333 (1993).
- [9] Y. Kubota *et al.* (CLEO II), Nucl. Instrum. Methods Phys. Res., Sec. A **320**, 66 (1992).
- [10] CLEO II Collaboration, R. Morrison *et al.*, Phys. Rev. Lett **67**, 1696 (1991).
- [11] Tomasz Skwarnicki, Ph.D. thesis, Institute of Nuclear Physics, Krakow, 1986, DESY internal report DESY F31-86-02 (unpublished).
- [12] H. Albrecht *et al.* (ARGUS), Phys. Lett. **B160**, 331 (1985).